EFDA–JET–CP(14)01/27

I. Bykov, H. Bergåker, G. Possnert, K. Heinola, J. Miettunen, M. Groth,
P. Petersson, A. Widdowson, J. Likonen and JET EFDA contributors

# Materials Migration in JET with ITER-Like Wall Traced with a $^{10}$Be Isotopic Marker

# Materials Migration in JET with ITER-Like Wall Traced with a $^{10}$Be Isotopic Marker

I. Bykov[1], H. Bergåker[1], G. Possnert[2], K. Heinola[3], J. Miettunen[4], M. Groth[4], P. Petersson[1], A. Widdowson[5], J. Likonen[6] and JET EFDA contributors*

***JET-EFDA, Culham Science Centre, OX14 3DB, Abingdon, UK***

*[1]Division of Fusion Plasma Physics, Association EURATOM-VR, Royal Institute of Technology KTH, Sweden*
*[2]Tandem Laboratory, Association EURATOM-VR, Uppsala Universitet, Box 256, Uppsala 75105, Sweden*
*[3]Department of Physics, University of Helsinki, P.O. Box 64, 00560 Helsinki, Association EURATOM-TEKES, Finland*
*[4]Aalto University, Association EURATOM-TEKES, 00076 Aalto, Finland*
*[5]EURATOM-CCFE Fusion Association, Culham Science Centre, OX14 3DB, Abingdon, OXON, UK*
*[6]Association EURATOM-TEKES, VTT, PO Box 1000, 02044 VTT, Espoo, Finland*
** See annex of F. Romanelli et al, "Overview of JET Results", (24th IAEA Fusion Energy Conference, San Diego, USA (2012)).*

Preprint of Paper to be submitted for publication in Proceedings of the
21st International Conference on Plasma Surface Interactions, Kanazawa, Japan
26th May 2014 - 30th May 2014

**ABSTRACT**

The current configuration of JET with ILW is the best available proxy for the ITER first wall. Be redistribution in JET ILW can be used for estimates of Be migration in ITER. To trace it, a localized isotopic Be marker has been implemented. The bulk $^{9}$Be tile has been enriched with $^{10}$Be by factor $10^5$, up to at concentrations of $1.7 \times 10^{-9}$. Prior to the start of the ILW campaign the marker tile has been installed at the inner midplane of JET.

During the 2012 shutdown over 100 surface samples were taken from limiter tiles from two toroidally opposite limiter beams. $^{10}$Be at concentration in each sample was measured with Accelerator Mass Spectrometry with sensitivity $\sim 10^{-14}$. The absolute areal densities of the marker were measured. The marker distribution was compared with predictions made with ASCOT, ERO and WallDYN codes. The simulations were able to partly reproduce the measured $^{10}$Be distribution pattern.

## 1. INTRODUCTION

Injection of isotopic markers has been used for tracking impurity transport in tokamaks. If a chemical element of interest forms volatile compounds with hydrogen or more exotic low- and medium-Z elements, the gas can be puffed in during a specific phase of the discharge or a series of discharges with similar plasma and magnetic configuration. The injection is normally done on the last days of operation prior to the tile exchange shut down in order to provide diagnostic access to the recent top most layers of the marker-containing deposits. Previously $WF_6$ has been used for measurement of W transport, $^{15}$N as a tracer of $^{14}$N [1, 2] and $^{13}$C-labeled methane for carbon transport studies [3]. A solid target ablated by laser impulse can also serve as a localized time selective impurity source [4]. Various Ion Beam Analysis (IBA) methods are used to measure marker concentration at the surface. Depth profiling in thick deposits is possible with Secondary Ion Mass Spectrometry (SIMS) [5]. $^{14}$C has also been proposed for marker experiments [6] as it can be measured with sensitivity about $5 \times 10^5$ at. employing Accelerator Mass Spectrometry, a well established method in radiocarbon dating applications.

## 2. EXPERIMENTAL

In JET with ITER-like wall the main material of the vessel protection is Be, thus it is possible to use the rarely occurring long lived isotope $^{10}$Be as a tracer of the majority impurity $^{9}$Be. The natural atomic concentration ratio of $^{10}$Be in Be ore is low because the only natural source of $^{10}$Be is the low rate spallation reactions of cosmic radiation on $^{14}$N and $^{16}$O in the upper atmosphere. $^{10}$Be decays with the half life $\tau = 1.4 \times 10^6$ yr., and in the ore with long geological history the at. fraction of $^{10}$Be is below $10^{-14}$. In a similar way as the measurements of the radio carbon markers are done, $^{10}$Be marker can be measured with sensitive Accelerator Mass Spectrometry (AMS) method. Its details in application to this experiment are described in [7]. The main advantage of AMS is in that the accelerator acts as a part of the spectrometer what makes it sensitive to at. concentrations of $^{10}$Be in

$^{9}$Be as low as $10^{-14}$. Another advantage of AMS is the possibility to separate $^{10}$Be from its abundant isobar $^{10}$B [7] present in JET at high concentration e.g. in BN insulators and thus potentially able to be sputtered and mixed with Be. Also due to the superior sensitivity of AMS the amount of Be in raw sample material can be in the low range 2100g. This made it possible to take samples non destructively from those tiles which had to be re-installed in the vessel and continue operation in the following ILW campaign.

The central section of one of the midplane IWGL limiters (cf. figure 3) in the ILW has been activated in a flux of thermal neutrals up to the $^{10}$Be/$^{9}$Be at. concentration ratio $1.73\text{x}10^{-9}$. The tile remained at its allocated position in IWGL during the campaign and has been temporarily removed for analysis in 2012 along with other 12 tiles. Six of them were removed from the same limiter beam (5Z) with the source tile, and another six came from the toroidally opposite limiter beam (2X), cf. figure 3. The sampling method has been purposely developed for the $^{10}$Be experiment at JET to collect the required 100g of material from IWGL tiles temporarily available during the 2012 shut down. The sampling procedure consisted in milling the top most layer with a rotating abrasive pad pressed to the tile surface, figure 1a. The changeable tip of the sampling tool was equipped with a sandpaper and a cushion pad to distribute the pressure more uniformly in case the surface was rough or the tool was not precisely aligned with the surface normal.

Collected material was dissolved in a 4M solution of HCl and undergone wet chemistry processing to separate and precipitate beryllium oxide. The oxide was then injected in the accelerator line by sputtering the Be target with Cs in the ion source of the AMS system. A known fraction of the initial solution was separated to measure the total content of $^{9}$Be in the sample by the ICP-MS method [8, pp. 21-23]. The chemical processing as well as the stages of isotopic separation of $^{10}$Be from interferences of which the main is $^{10}$B, are described in [7, 9].

### *2.1 SELECTION OF MATERIALS FOR SAMPLING.*

Preliminary tests were conducted to select an appropriate type and grit of the sandpaper and to define the regime to operate the sampling tool. Most important was to ensure that the amount of scratched Be is in the range 100m, as required for AMS sensitivity.

Use of Be in laboratory tests, especially when ne dust is produced, is limited due to its toxicity. Frequently used surrogates for Be are Al and Mg [10]. As the material has to be sampled by abrasive scratching, the figure of merit is the mechanical properties of the proxy. The ability of a material to be scratched is characterized by the Mohs hardness, which for Be, Al and Mg equals respectively 5.5, 2.75 and 2.5. From this perspective, a better alternative can be Si with Mohs hardness 7, implying that it is easier to scratch Be than Si. We used polished Si wafers to test the sampling method also because their low original surface roughness made it easy to characterize the surface modification due to scratching. The roughness has been assessed with profilometry before and after the test-sampling. Keeping the introduced roughness within 10μm was another requirement for the method.

Based on the tests with Si wafers a P600 SiC sandpaper was selected, which demonstrated the

lowest Be background compatible with the declared sensitivity of the AMS measurements of $^{10}$Be, ability to collect sufficient amount of material and acceptable residual roughness of the sampled surface. It was found that with applied pressure 30.5kgf/cm$^2$ ≃0.05MPa the sandpaper saturated with scratched material after less than 20 turns of the sampling head and further scratching was greatly reduced. The removed material stuck in the gaps between grits and did not sink. Hence, after the saturation the thickness of removed layer was defined by the sandpaper grit. An equivalent mass of Be that could be collected was estimated assuming the same volume available for a sampled material in the sandpaper and accounting for difference in the density between Si and Be. The thickness of the layer affected by the sandpaper was a few microns. After the tests done on smooth surfaces it was expected that a large scale surface roughness produced during plasma operation could affect the efficiency of material removal. Also the thickness of the removed surface could increase if the sampling spot had smaller area.

The size of a sample spot and hence the amount of collected material is limited by the design of the IWGL limiters, figure 1a. Bulk Be tiles were sliced in order to suppress eddy currents. The plasma facing surface of each tile was additionally castellated to ensure integrity under spatially non uniform heating. The size of the castellation is 12x12mm$^2$ with sub mm gaps between them, figure 1b. The requirement was that the removed material is not transported into the castellation gaps and the castellation edges are not scratched. Also the scratched material had to be removed from the surface completely to avoid Be dust on the limiter surfaces. No wet cleaning was permitted. The requirements were met by using an extra holder for tiles keeping them in upright position with a slight tilt towards the plasma facing surface so that the dust could not fall into the gaps, and loose clusters stayed on the sandpaper. The size of the sampling head was ø10 mm, sufficient to keep it 31 mm from the castellation edges (cf. figure 1) and collect ~100g of Be.

**RESULTS AND DISCUSSION**

Over 100 positions were sampled at the surfaces of IWGL limiters from two toroidally opposite beams. On the tiles far from the source in the beam 5Z (cf. figure 3) the pattern consisted of 4 points distributed uniformly along the tile, while the source and the two contiguous tiles were covered by a denser grid of points, figure 1b. In many cases additional samples were taken in various locations including side and back surfaces of the tiles.

Examples of the sampling spots' appearance are shown in figure 2. In most cases (a, b) the spot is round, of the same size as the sampling head, and the material is probed from a thin layer at the surface. When the tile surface is affected by arc trenches (b) or has a resolidified melt layer (d) its roughness increases. Thus, the effective sample area is reduced because the sandpaper does not reach the deeps in the surface. This reduction could partly be accounted for by measuring the area of sampled spots.

AMS measures a scaled ratio $R_s$ of $^{10}$Be and $^{9}$Be atomic concentrations in the sample. The actual atomic fraction $C_{10Be}$ of $^{10}$Be can be recovered if a standard with known isotopic content

$C_{st}$ of $^{9}$Be is measured in the same experiment: $C_{10Be} = {}^{R_s}/_{F_{irst}}\, C_{st}$. In order to control possible cross contamination several blank Be samples with known low content of $^{9}$Be were prepared in the same process and measured along with the real samples. No contamination was detected. Assuming that the sampling depth was larger than the thickness of deposited layers, we calculate the areal density of $^{10}$Be as: $N_{10Be} = C_{10Be} \cdot M/S$, where M is the total amount of Be in the sample and S is the area of the sample spot. S is measured from photographs of the spots. In most cases the spot size could be identified with accuracy better than 20%, see figure 2a, b. But in measurements on rough surfaces, cf. figure 2c, d, the area estimate could introduce the major error up to 50%.

The main findings of the $^{10}$Be areal density measurements in different locations on the tile surfaces are following:

- Visually thick deposits were found on the side surfaces of the tiles, where the sampling depth could be lower than the layer thickness and hence the measurement underestimated 10Be areal density. These deposits had in all cases low $^{10}$Be/$^{9}$Be ratio ~$1x10^{-12}$, thus, the total unaccounted areal density of $^{10}$Be in those areas was low.
- Considerable concentrations of the marker ~$10^{7}$ $^{10}$Be/cm$^2$ were measured in net erosion zones in the central parts of the limiters [11]. This is higher than what would be expected if 10Be concentration were defined by dynamic equilibrium between implantation and net erosion. Thus, it may be important to include other mechanisms of Be mixing in the simulations of surface evolution [12].
- A noticeable concentration of $^{10}$Be $3x10^{6}$ at./cm$^2$ was measured at two close positions at the back side of the bottom tile in the beam 2X far from the source. Conversely, there is a factor 100 dilution of the marker at the back side of the source tile compared to its original activation. The reduction of the $^{10}$Be concentration must be due to a non local transport of $^{9}$Be either from the non activated wings of the source tile or from remote tiles.
- In order to assure credibility of the results samples taken from adjacent locations were prepared and measured independently. Far from the source the marker density gradients are expected to be low what was confirmed by the measurements, see for example vertically adjacent spots on tiles 5 and 14, beam 2X.

It could be expected there to be no deposition at shadowed areas at the back sides of the tiles and there the $^{10}$Be concentration could be a measure of the background. The measured concentrations were, nevertheless, 420% higher than the minimum marker density measured at the plasma facing side of the limiters. Due to an inconvenient access to the back side of the tile the areas of the sample spots differed by factor of three and the total $^{10}$Be content measured varied accordingly. This proportionality suggests that the marker was contained in a surface layer rather than in bulk material. This finding helps to exclude the activation of $^{9}$Be by capturing D-D neutrons as a source of $^{10}$Be background.

### *3.1 EFFECTS OF SURFACE MELTING.*

Besides the atomic sputtering the limiter tiles including the marker source can experience local melting and arcing which leads to material evaporation, ejection of droplets and mixing in the melt layer. Signatures of these processes were observed on the surfaces of the IWGL tiles [13]. The source intensity would decrease if the $^{10}$Be-enriched bulk material mixes at the surface with deposited $^{9}$Be. In net deposition zones the source intensity would drop after initial deposition of few $10^{16}$ at./cm$^2$ of $^{10}$Be-poor material. In net erosion zones on the marker tile surface a dynamic balance of deposition and erosion fluxes would lead to a (slight) dilution of the source. This effect is expected to be insignificant, and the actual $^{10}$Be at. concentration at the marker surface will be measured later in the samples which have been taken (figure 3b).

### *3.2 COMPARISON WITH MODELLING.*

The main complication in simulating marker migration for comparison with the measurements is in that the marker distribution is campaign integrated and is not specific for any particular discharge phase or scenario. This complicates modelling which is bound to specific plasma conditions normally taken from one or few reference discharges, not representing the whole campaign. Extra complications arise if, for example, in the beginning of the campaign the source tile experienced arcing or local melting. This could lead to enhanced erosion unaccounted by spectroscopy. Should the droplets be ejected and redeposited outside the marker tile, they will act as an extra source of $^{10}$Be. Visual inspection of the marker tile made during the sampling did not reveal any considerable damage to the source tile, except few arc traces preferentially localized at the bottom right of the source.

Regardless the possible marker dilution at the surface, a reliable total amount of eroded $^{10}$Be can be inferred from volumetric reduction of the source tile. This is calculated after a surface profilometry survey done before and after the ILWcampaign on IWGL tile 10 in the beam 2X [11]. The measured amount of eroded Be was 50.8g which corresponds to $10^{14}$ atoms of $^{10}$Be. Preliminary results of quantitative marker mapping in net deposition zones of IWGLs were presented in [14] and led to conclusion that even the upper-bound estimated integrated amount of collected 10Be only accounts for 2% of the eroded amount. Adding the new data from erosion zones of IWGLs and from the sides of the tiles changes this number by less than 1%. The rest must be deposited outside the IWGLs. Possible locations are the horizontal surfaces below the IWGL beams accessible by the plasma in limiter modes and containing thick deposits of Be [15]. These areas are suggested as a main Be sink also by simulations with the WallDYN code [16, 17] and the 3D ERO code [18] considering Be migration in divertor phases of the discharges. In [19] the absolute Be deposition in the inner divertor areas was taken as an input for ERO simulation to match the expected erosion source of Be at the IWGL during the divertor operation. The obtained value must be considerably underestimating net IWGL erosion which is dominated by limiter operation and hence most of redeposited Be (along with eroded 10Be marker) must be residing in the main chamber.

A first-flight simulation of marker redistribution was done with the 3D orbit following code

ASCOT, reproducing the details of 3D geometry of the JET wall. The details of the simulation can be found in [20]. Figure 3 shows a comparison of measured and predicted marker distribution on the IWGL beams 2X and 5Z. The simulation was done only for the limiter discharge phases and does not predict any considerable transport of Be towards the divertor. This is in contradiction with the above mentioned spectroscopy evidence of predominant Be erosion in the limiter phases and the low net deposition measured with profilometry on the wings of the IWGL limiters [11]. Previously the simulation was also done for the divertor mode assuming initial marker distribution acquired during the limiter operation. The modelling also predicted main marker deposition on the upper horizontal surfaces of the divertor, cf. figure 4 in [20]. Notably, in this simulation the marker tile was \switched off, therefore it is difficult to compare the results with the measurements.

The simulated marker deposition on IWGLs reproduced some features of the measured distribution, see figure 3. On the beam 2X the marker density peaks at the rhs of tile 14 consistently with the modelling. At this position two close samples were taken and processed independently in different batches. They credibly showed equal high marker concentration. Also there is in average higher deposition on the beam 2X above the mid plane compared to its lower part. On the beam 5Z the marker concentration locally peaks at the bottom left part coherently with the modelling. The sampling frequency may be insufficient to recover the details. The area around the source tile was sampled more densely and the measurements confirmed the modelling prediction of higher local deposition above the source. The local left right asymmetry is not well reproduced by ASCOT and has to be a subject of more detailed simulation e.g. by the ERO code [21].

In general, on most tiles the strong left-right asymmetry suggested by ASCOT modelling is not supported by the measurement, and in some cases (e.g. upper part of the beam 5Z) the measured asymmetry is opposite. The typical S-shaped patterns of deposition favoring the upper right and bottom left sides of the limiter beams (see figure 1 in [22]) are formed in the model maps due to the large expected fraction of the marker penetrating into the core and diffusing into the SOL. This pattern is hindered in the measured marker distribution. Apart from the fact that the simulation was done for the limiter phases, the reason for the discrepancies may be a stronger Scrape-off Layer (SOL) transport than that assumed in the simulation and impact of the SOL flows [19].

## CONCLUSIONS

The areal density of $^{10}$Be marker transported from a localized source has been measured after the first period of ILW operation through 2011-2012. The concentration maps were obtained for two toroidally opposite IWGL beams with poloidal and toroidal resolution. Far from the source the marker deposition favoured the deposition-dominated wings of the tiles. A considerable deposition was also found in net erosion zones in central parts of the tiles. The measured asymmetries could partly be reproduced by a 3D numerical simulation with ASCOT and did not contradict to the ERO and WallDYN expectations of predominant $^{9}$Be migration towards the apron of the divertor Tile 1. The comparison will be extended by including measurements on the divertor surfaces. The local

poloidal asymmetry of marker redeposition around the source is in qualitative agreement with the ASCOT modelling. Spatial resolution of the measurements around the source permits more detailed comparison with local transport predictions which can be done e.g. with ERO code.

**ACKNOWLEDGEMENTS.**

This work was supported by EURATOM and carried out within the framework of the European Fusion Development Agreement. The views and opinions expressed herein do not necessarily reflect those of the European Commission.

**REFERENCES**

[1]. P. Petersson, M. Rubel, G. Possnert, et al. Nuclear reaction and heavy ion ERD analysis of wall materials from controlled fusion devices: Deuterium and nitrogen-15 studies. Nuclear Instruments and Methods in Physics Research Section B: Beam Interactions with Materials and Atoms, **273**:113–117, 2012. 20th International Conference on Ion Beam Analysis.

[2]. P. Petersson, A. Hakola, J. Likonen, et al. Injection of nitrogen-15 tracer into ASDEX-Upgrade: New technique in material migration studies. Journal of Nuclear Materials, **438**, Supplement:S616–S619, 2013. Proceedings of the 20th International Conference on Plasma-Surface Interactions in Controlled Fusion Devices.

[3]. A. Hakola, J. Likonen, L. Aho-Mantila, et al. Migration and deposition of 13C in the full-tungsten ASDEX Upgrade tokamak. Plasma Physics and Controlled Fusion, **52**(6):065006, 2010.

[4]. K.W. Gentle. Diagnostics for magnetically conned high-temperature plasmas. Reviews of Modern Physics, **67**:809–836, 1995.

[5]. J.D. Strachan, J. Likonen, P. Coad, et al. Modelling of carbon migration during JET 13C injection experiments. Nuclear Fusion, **48**(10):105002, 2008.

[6]. M. J Rubel, J.P Coad, K Stenström, et al. Overview of tracer techniques in studies of material erosion, re-deposition and fuel inventory in tokamaks. Journal of Nuclear Materials, **329–333**, Part A:795–799, 2004. Proceedings of the 11th International Conference on Fusion Reactor Materials (ICFRM-11).

[7]. Igor Bykov. Experimental studies of materials migration in magnetic connement fusion devices. PhD thesis, Royal Institute of Technology (KTH), 2014.

[8]. R. Ekman, J. Silberring, A. Westman-Brinkmalm, and A. Kraj, editors. Mass Spectrometry: Instrumentation, Interpretation, and Applications. Wiley, 2009.

[9]. Ann-Marie Berggren. Influence of solar activity and environment on 10Be in recent natural archives. PhD thesis, Uppsala Universitet, 2009.

[10]. Laurent Marot, Christian Linsmeier, Baran Eren, et al. Can aluminium or magnesium be a surrogate for beryllium: A critical investigation of their chemistry. Fusion Engineering and Designs, **88**(9-10):1718–1721, 2013. Proceedings of the 27th Symposium On Fusion Technology (SOFT-27); Liege, Belgium, September 24-28, 2012.

[11]. K. Heinola, C.F. Ayres, A. Baron-Wiechec, et al. Tile profiling analysis of samples from the jet iter-like wall and carbon wall. Physica Scripta, **T159**:014013, 2014.

[12]. K. Schmid. Implementation of a diusion convection surface evolution model in WallDYN. Journal of Nuclear Materials, **438**, Supplement(0):S484–S487, 2013. Proceedings of the 20th International Conference on Plasma-Surface Interactions in Controlled Fusion Devices.

[13]. A. Widdowson, E. Alves, C.F. Ayres, et al. Material migration patterns and overview of first surface analysis of the JET iter-like wall. Physica Scripta, **T159**:014010, 2014.

[14]. H. Bergaker, G. Possnert, I. Bykov, et al. First results from the $^{10}$Be marker experiment in JET with ITER like wall. Nuclear Fusion.

[15]. A. Baron-Wiechec, A. Widdowson, E Alves, et al. Global erosion patterns in JET with the ITER-like wall. This conference.

[16]. M. Reinelt, K. Krieger, S. Lisgo et.al. Journal of Nuclear Materials, **415**:S305–S309, 2011.

[17]. K. Krieger. Private communication, 2013.

[18]. A. Kirschner, V. Philipps, J. Winter, and U. Kögler. Simulation of the plasma-wall interaction in a tokamak with the Monte Carlo code ERO-TEXTOR. Nuclear Fusion, **40**(5):989, 2000.

[19]. M. Airila, A. Järvinen, M. Groth, and P. Belo. Beryllium migration during JET ITER-Like Wall divertor operation. These proceedings.

[20]. J. Miettunen, M. Groth, T. Kurki-Suonio, and H. Bergaker. Journal of Nuclear Materials, **438**:S612–S615, 2013.

[21]. D. Borodin, A. Kirschner, S. Carpentier-Chouchana et al. Physica Scripta, **T145**:014008, 2011.

[22]. G.F. Matthews, M. Beurskens, S. Brezinsek, et al. JET ITER-Like Wall overview and experimental programme. Physica Scripta, 2011(**T145**):014001, 2011.

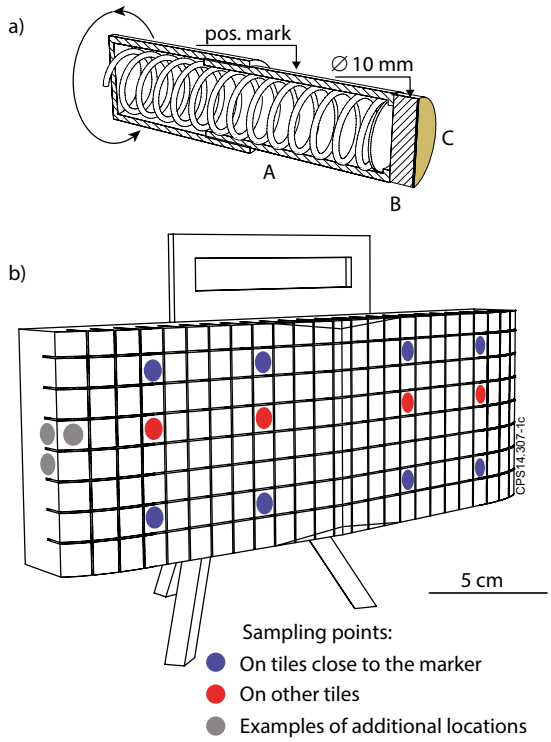


*Figure 1. (a) Construction of the sampling tool. The spring loaded pin A is pressed towards the tile surface and rotated given number of times similar for all samples. A position mark on the pin serves to achieve similar pressure in each collection. The pin is equipped with accessory head with ~2 mm thick cushion pad B with abrasive layer C on its top. (b) shows tile xation during the sampling: the plasma facing surface is nearly vertical with slight negative tilt to avoid dust dropping in the gaps. Standard sampling positions are shown in color.*

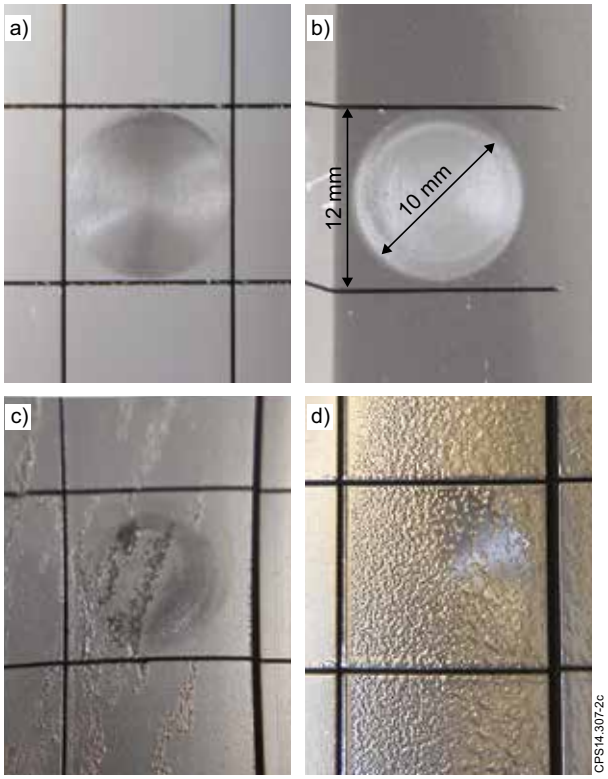


*Figure 2. Examples of surface appearance before and after the abrasive sampling. (a, b) show typical spots and area around them observed in most cases. (c, d) illustrate a reduction of the spot size due to excessive surface roughness.*

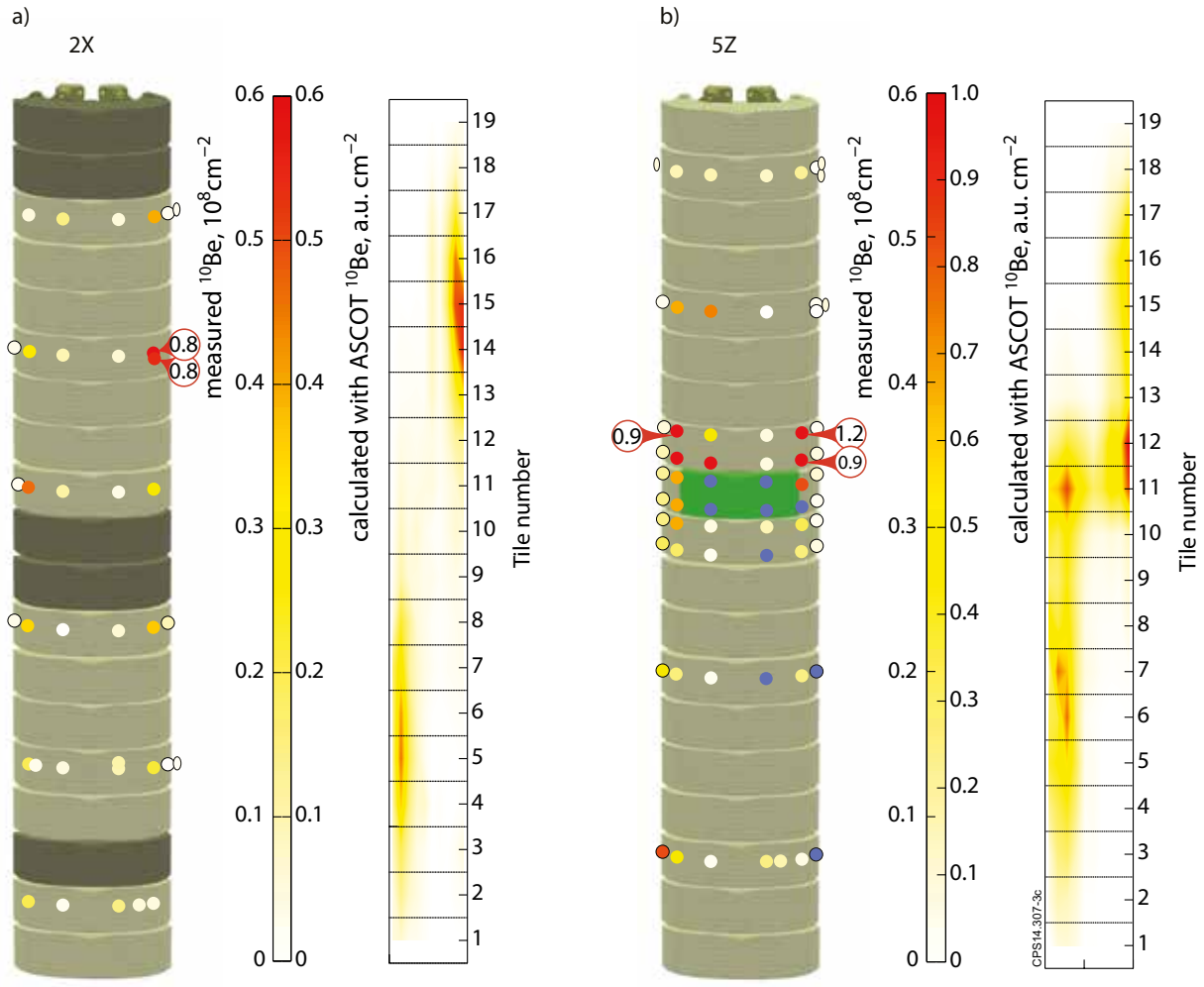


*Figure 3. Marker deposition patterns on the IWGL limiters in the two toroidally opposite beams: 2X shown in (a) and 5Z in (b). Each spot corresponds to one measurement, the spot size is exaggerated for better display. Side labels indicate measured $^{10}$Be values falling beyond the color bar maximum. Spots drawn outside the markers were taken from the side surfaces. Blue-lled spots indicate failed samples except the source samples (on the central tiles of IWGL 11 in the beam 5Z), which have not been processed yet. In each case the measured areal densities of $^{10}$Be are compared with expected dimensionless distribution obtained by ASCOT simulation.*